

Noise generated by cavitating single-hole and multi-hole orifices in a water pipe

P. Testud^{a,*}, P. Moussou^a, A. Hirschberg^b, Y. Aurégan^c

^aLaboratoire de Mécanique des Structures Industrielles Durables, UMR CNRS-EDF 2832, 1 Avenue du Général De Gaulle, F-92141 Clamart, France

^bFluid Dynamics Laboratory, Department of Applied Physics, Technische Universiteit Eindhoven, P.O. Box 513, 5600 MB Eindhoven, The Netherlands

^cLaboratoire d'Acoustique de l'Université du Maine, UMR CNRS 6613, Avenue Olivier Messiaen, F-72085 Le Mans Cedex 9, France

Received 13 December 2005; accepted 5 August 2006
Available online 27 October 2006

Abstract

This paper presents an experimental study of the acoustical effects of cavitation caused by a water flow through an orifice. A circular-centered single-hole orifice and a multi-hole orifice are tested. Experiments are performed under industrial conditions: the pressure drop across the orifice varies from 3 to 30 bar, corresponding to cavitation numbers from 0.74 to 0.03. Two regimes of cavitation are discerned. In each regime, the broadband noise spectra obtained far downstream of the orifice are presented. A nondimensional representation is proposed: in the intermediate 'developed cavitation' regime, spectra collapse reasonably well; in the more intense 'super cavitation' regime, spectra depend strongly on the quantity of air remaining in the water downstream of the orifice, which is revealed by the measure of the speed of sound at the downstream transducers. In the 'developed cavitation' regime, whistling associated with periodic vortex shedding is observed. The corresponding Strouhal number agrees reasonably well with literature for single-phase flows. In the 'super cavitation' regime, the whistling disappears.

© 2006 Elsevier Ltd. All rights reserved.

Keywords: Confined flow; Orifice; Cavitation; Broadband noise; Whistling

1. Introduction

1.1. Motivations

In industrial processes, cavitating flows are known to sometimes generate significant levels of noise and high vibrations of structures. Some papers have been published in the last years on this topic: Au-Yang (2001), Weaver et al. (2000), Moussou (2004).

In particular, fatigue issues have been reported recently for the configurations of a cavitating valve (Moussou et al., 2001) and a cavitating orifice (Moussou et al., 2003). The examination of the noise generated by a cavitating device, in

*Corresponding author.

E-mail address: philippe.testud@edf.fr (P. Testud).

Nomenclature			
c	speed of sound measured downstream of the orifice (in m s^{-1})	U_j	volume flux divided by orifice jet cross-sectional area (in m s^{-1})
c_w	speed of sound in pure water (in m s^{-1})	G_{pp}	Power spectrum density of the pressure (in Pa^2/Hz)
c_{\min}	minimum speed of sound (in m s^{-1})	N_{holes}	number of holes for the multi-hole orifice ($N_{\text{holes}} = 47$)
d	diameter of the single-hole orifice ($d = 2.2 \times 10^{-2}$ m)	p^+, p^-	forward, backward propagating plane wave spectra (in $\text{Pa}/\sqrt{\text{Hz}}$)
d_{eq}	single-hole equivalent diameter of the multi-hole orifice ($d_{\text{eq}} = 2.1 \times 10^{-2}$ m)	P_1, P_2	static pressure, respectively, upstream and far downstream of the orifice
d_{multi}	diameter of the holes of the multi-hole orifice ($d_{\text{multi}} = 3 \times 10^{-3}$ m)	P_j	static pressure at the jet (vena contracta)
f_0	whistling frequency (in Hz)	P_v	vapor pressure ($P_v(310 \text{ K}) = 5.65 \times 10^3$ Pa (Tullis, 1989))
D	pipe diameter ($D = 7.4 \times 10^{-2}$ m)	S	cross-section of the pipe (in m^2)
S_j	cross section of the jet (in m^2)	ΔP	static pressure difference across the orifice (in Pa)
St	Strouhal number for the whistling frequency	ν_{water}	kinematic viscosity of water [$\nu_{\text{water}}(310 \text{ K}) = 7.2 \times 10^{-7}$ $\text{m}^2 \text{ s}^{-1}$ (Idel'cik, 1969)]
t	orifice thickness, ($t = 14 \times 10^{-3}$ m)	β	volume fraction of gas in the water
t_p	pipe wall thickness ($t_p = 8 \times 10^{-3}$ m)	ρ_w	density of water ($\rho_w(310 \text{ K}) = 994$ kg m^{-3})
U	volume flux divided by pipe cross-sectional area (in m s^{-1})	σ	cavitation number
U_d	volume flux divided by orifice cross-sectional area (in m s^{-1})	σ_i	incipient cavitation number
		σ_{ch}	choked cavitation number

this study a cavitating orifice, is typically an industrial issue. It provides information which is a basis for a safer design in terms of pipe vibrations.

1.2. Literature

In single-phase flow, an orifice generates a free jet surrounded by a dead water pressure region of uniform pressure, cf. Fig. 1. The static pressure reaches its minimum value P_j in the jet region, also called the vena contracta, and large eddies are generated in the shear layer separating the jet from the dead water region.

Two-phase flow transition occurs when the lowest static pressure in the fluid falls below the vapor pressure (Brennen, 1995). The level of cavitation is usually correlated with the help of a so-called cavitation number. Different definitions exist of the cavitation number for cavitation in a flowing stream (also called hydrodynamic cavitation). They correspond to different cavitation configurations, and are usually chosen for convenience, so that they can easily be determined in practice:

- (i) For wake cavitation, that is cavitation round a body (i.e. an hydrofoil) or generated by a slit, the cavitation number is commonly defined as function of the upstream conditions (Young, 1999; Brennen, 1995; Franc et al., 1999; Lecoffre, 1994):

$$\sigma = \frac{P_0 - P_v}{(1/2)\rho_L U_0^2}, \quad (1)$$

where U_0 is the infinite upstream flow velocity, P_0 the ambient static pressure, P_v the vapor pressure of the liquid and ρ_L the density of the liquid.

- (ii) For mixing cavitation, that is cavitation formed in a jet (i.e. in pumps, valves, orifices), a similar cavitation number, as in the wake cavitation, can be used (Young, 1999; Brennen, 1995):

$$\sigma = \frac{P_{\text{ref}} - P_v}{(1/2)\rho_L U_0^2}, \quad (2)$$

where P_{ref} is very often defined as the downstream static pressure.

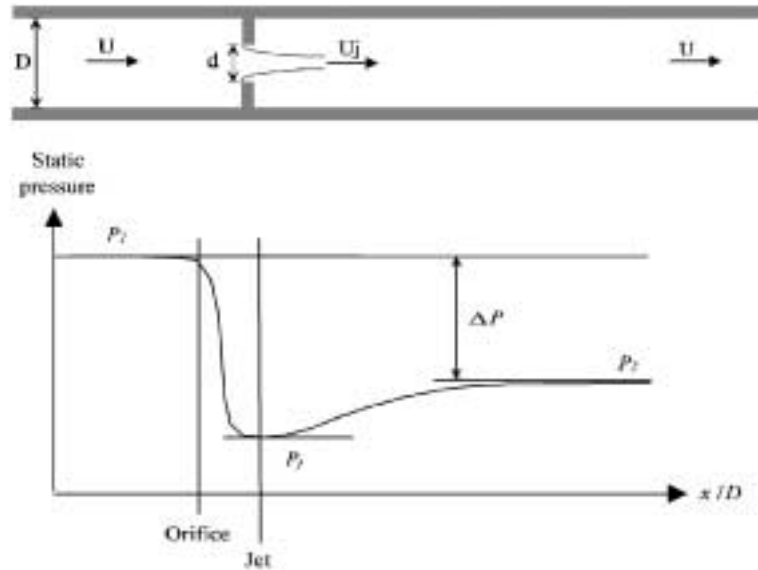


Fig. 1. Flow through an orifice and corresponding evolution of the static pressure.

We prefer to use the cavitation number, based on the pressure drop across the singularity generating the jet:

$$\sigma = \frac{P_2 - P_v}{\Delta P}, \quad (3)$$

where $\Delta P = P_1 - P_2$ is the pressure drop across the orifice, with P_1 the static pressure upstream of the orifice and P_2 the downstream static pressure far away from the orifice. In this choice, we follow common practice in industry (Tullis, 1989; Franc et al., 1999; Lecoffre, 1994).

One should note that both those cavitation numbers lead to very similar classifications as they are related to each other by the pressure drop coefficient of the singularity.

When the pressure P_j has a sufficiently low value, intermittent tiny cavitation bubbles are produced in the heart of the turbulent eddies along the shear layer of the jet. This flow regime transition is called cavitation inception, and it appears at a cavitation number of the order of 1 (when $d/D = 0.30$) according to the data of Tullis (1989). Other references (Numachi et al., 1960; Tullis and Govindajaran, 1973; Ball et al., 1975; Yan and Thorpe, 1990; Kugou et al., 1996; Sato and Saito, 2001; Pan et al., 2001) are in good agreement with the values and scale effects given by Tullis (1989). Some differences result from the influence of the variation in the dissolved gas content and in the viscosity (Keller, 1994).

As the jet pressure decreases further, more bubbles with larger radii are generated, forming a white cloud. The pressure fluctuations increase and a characteristic shot noise can be heard. A further decrease in jet pressure induces the formation of a large vapor pocket just downstream of the orifice, surrounding the liquid jet. The regime occurring after this transition is called super cavitation and it exhibits the largest noise and vibration levels. In the super cavitation regime, noise is known [see, for example, Van Wijngaarden (1972)], to be mainly generated in a shock transition between the cavitation region and the pipe flow, at some distance downstream of the orifice. Downstream of the shock, some residual gas (air) bubbles can persist but pure vapor bubbles have disappeared.

Cavitation indicators are used to predict the occurrence of cavitation regimes. The use of two of them has seemed relevant, in view of our experimental results. First, a so-called incipient cavitation indicator, noted σ_i , which predicts the transition from a noncavitating flow to a moderately cavitating flow, that is called developed cavitation regime. Second, a so-called choked cavitation indicator, noted σ_{ch} , which predicts the transition from a moderately cavitating flow to a super cavitating flow, with the formation and continuous presence of a vapor pocket downstream of the orifice around the liquid jet. To calculate both those incipient and the choked cavitation indicators, scaling laws are given by Tullis (1989). They take into account the various pressure effects and size scale effects, by means of extensive experiments on single-hole orifices in water pipe flow. For multi-hole orifices, as mentioned in the same work, less data are available but identical values are expected to hold.

Only a few studies provide downstream noise spectra generated by cavitating orifices (Yan et al., 1988; Bistafa et al., 1989; Kim et al., 1997; Pan et al., 2001). A few complementary studies give the noise spectra created by cavitating valves

(Hassis, 1999; Martin et al., 1981). In fact, it appears that far more research has been developed on submerged water jets (Jorgensen, 1961; Esipov and Naugol'nykh, 1975; Franklin and McMillan, 1984; Brennen, 1995; Latorre, 1997). A comprehensive overview of the state of the art in this domain is given in Brennen (1995).

2. Experimental set-up

2.1. Tested orifices

In the piping system of French nuclear power plants, a basic configuration to obtain a pressure discharge can be realized with a single-hole orifice. The maximum flow velocity can reach about 10 m s^{-1} and the pressure drop 100 bar across the orifice. This can induce high vibration levels. The orifices used are chosen in order to reduce the pipe vibration to acceptable levels (Caillaud et al., 2006).

In our study, two orifices have been tested (see Fig. 2), as follows:

- (i) A single-hole orifice, circular, centered, with right angles and sharp edges. It has a thickness of $t = 14 \text{ mm}$ ($t/d = 0.64$) and a diameter of $d = 22 \text{ mm}$ ($d/D = 0.30$), for a pipe diameter of $D = 74 \text{ mm}$. It is considered as a 'thin' orifice as $t/d \lesssim 2$ (Idel'cik, 1969). In a sharp edged orifice flow, separation occurs at the upstream inlet edge. In a thin orifice, there is no reattachment of the flow within the orifice.
- (ii) A multi-hole orifice, with $N_{\text{holes}} = 47$ circular right-angled and sharp-edged perforations of diameter $d_{\text{multi}} = 3 \text{ mm}$. Its total open surface is practically identical to the single-hole orifice one, as it has an equivalent $d_{\text{eq}}/D = 0.28$ ratio. This multi-hole orifice also has the same thickness of $t = 14 \text{ mm}$ ($t/d_{\text{multi}} = 4.67$). It behaves as a thick orifice $t/d \gtrsim 2$. The flow reattaches to the wall within the orifice.

2.2. Test rig

The test-section, as shown in Fig. 3, consists out of an open loop with a hydraulically smooth steel pipe of inner diameter $D = 74 \text{ mm}$ and wall thickness $t_p = 8 \text{ mm}$. The orifices are placed between straight pipe sections with lengths, respectively, equal to 42 diameters upstream and 70 diameters downstream.

The water is injected from a tank located 17 m upstream from the orifice. The nitrogen pressure in the tank above the water is controlled by a feedback system to maintain a constant main flow velocity. The water is released at atmospheric pressure 20 m downstream of the orifice. The temperature is kept equal to 310 K ($\pm 1 \text{ K}$) during all experiments.

The flow velocity U is measured $26D$ upstream of the orifice, and the static pressures P_1 and P_2 are determined, respectively, by a transducer $11D$ upstream and another $40D$ downstream of the orifice. The fluctuating pressures are monitored by means of a combination of Kistler 701A piezo-electrical transducers and Kistler charge amplifiers. The location of the dynamical pressure transducers is given in Fig. 4. Upstream, the transducers 1–3 are positioned, at respectively $11D$, $8D$ and $5D$ from the orifice (0.25 m between consecutive transducers). Downstream, the transducers 4–10 are regularly positioned, from $7D$ to $39D$ (0.4 m between consecutive transducers).



Fig. 2. Front views of the tested orifices: (a) single-hole orifice; (b) multi-hole orifice.

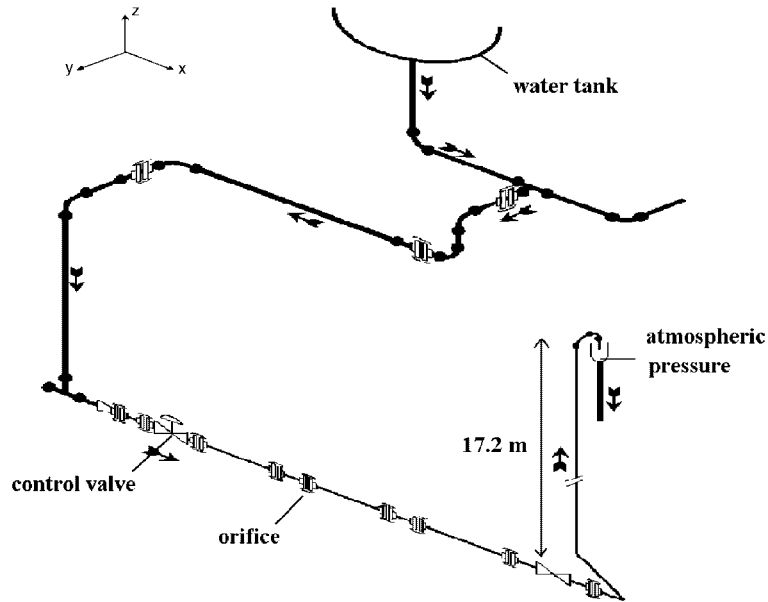


Fig. 3. Scale scheme of the test rig.

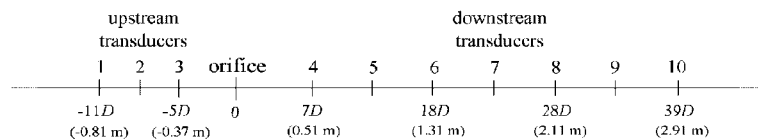


Fig. 4. Location of the dynamical pressure transducers upstream and downstream of the orifice.

2.3. Experimental conditions

2.3.1. Water quality

The water used is tap water, demineralized, with pH 9 and weak conductivity. It is not degassed, hence it is expected to be saturated with dissolved air. The volume fraction of dissolved gas (denoted by β) is high compared to other cavitation studies. This gas content has not been measured, but an estimation, assuming saturation condition under a temperature of $T = 310 \text{ K}$ or $T = 273 \text{ K}$, gives for the volume fraction an order of magnitude around, respectively, 10^{-2} or 10^{-3} .

It should be pointed out that the presence of dissolved gas in the water does not mean a presence of gas bubbles in the water. Thus, the measured upstream speed of sound does not reveal any presence of gas bubbles as it is close to the one in pure water flow.

Correcting the compressibility of the water for the influence of the elasticity of the pipe (diameter $D = 7.4 \times 10^{-2} \text{ m}$, wall thickness $e = 8 \times 10^{-3} \text{ m}$, Young's modulus $E = 2 \times 10^{11} \text{ N m}^{-2}$, Poisson ratio $\zeta = 0.3$), the speed of sound c_{th} in pure water in the pipe is given in function of the speed of sound in pure water c_w (Lighthill, 1978):

$$c_{th} = c_w \left(1 + \rho_w c_w^2 \frac{D(1 - \zeta^2)}{eE} \right)^{-0.5} \quad (4)$$

This predicts a speed of sound of $c_{th} = 1454 \text{ m s}^{-1}$ using $c_w = 1523 \text{ m s}^{-1}$. The measured speed of sound upstream of the orifice is $1420 \pm 10 \text{ m s}^{-1}$.

2.3.2. Experimental flow conditions

Experiments are carried out at a constant flow by controlling the static pressure upstream of the orifice. The downstream pressure P_2 is imposed by the hydraulic static head of the 17.2 m high vertical pipe downstream of the

orifice. Each experiment lasts about 90 s. Pressures and volume flows are provided in Table 1 for the six experiments on the single-hole orifice, and in Table 2 for the six experiments on the multi-hole orifice.

The Reynolds number $Re = UD/\nu_{\text{water}}$ based on the pipe diameter and the water viscosity varies from 2×10^5 to 5×10^5 ; turbulence is fully developed, as usual in industrial pipes.

Higher flow regimes have been tested, but the pressure transducers downstream delivered no signal, as they were located in a vapor pocket characteristic of the super cavitation regime. As a consequence, no acoustic data are available in these conditions, and the corresponding hydraulic conditions are not reported in Tables 1 and 2.

2.4. Distinction of two cavitation regimes

The application of Tullis' formulas to our experiments gives the cavitation indicators: σ_i for the developed cavitation and σ_{ch} for the super cavitation. Compared to our observations, those cavitation regime indicators are in good agreement:

- (a) For the single-hole orifice: $\sigma_i \geq 0.93$, $\sigma_{\text{ch}} = 0.25$. The observations, based on listening and on the measured downstream speed of sound, indicate that all experiments (i.e. $\sigma < 0.74$) are cavitating. Furthermore, the downstream acoustic properties and particularly the shape of the downstream noise spectra indicate that the last three experiments (i.e. $\sigma < 0.25$) are in super cavitation regime.
- (b) For the multi-hole orifice: $\sigma_i \geq 0.87$, $\sigma_{\text{ch}} = 0.20$. The observations in this case indicate that all experiments (i.e. $\sigma < 0.74$) are cavitating. The super cavitation regime is observed for the last two experiments (i.e. $\sigma < 0.17$).

Table 1
Flow conditions for the single-hole orifice experiments (with standard deviations)

	Developed cavitation			Super cavitation		
U (m s ⁻¹)	1.91	2.38	2.90	3.75	4.08	4.42
St. deviation (m s ⁻¹)	0.06	0.04	0.04	0.03	0.03	0.05
P ₁ (10 ⁵ Pa)	6.3	9.2	13.3	21.4	25.0	29.5
St. deviation (10 ⁵ Pa)	0.3	0.3	0.6	1.4	0.7	0.8
P ₂ (10 ⁵ Pa)	2.7	2.7	2.7	2.8	2.8	2.8
St. deviation (10 ⁵ Pa)	0.0	0.0	0.0	2.0	0.2	1.5
σ	0.74	0.41	0.25	0.15	0.12	0.10

Table 2
Flow conditions for the multi-hole orifice experiments (with standard deviations)

	Developed cavitation			Super cavitation		
U (m s ⁻¹)	2.08	2.45	2.94	3.65	4.18	4.43
St. deviation (m s ⁻¹)	0.02	0.04	0.04	0.02	0.02	0.04
P ₁ (10 ⁵ Pa)	6.5	6.9	12.9	19.8	26.0	28.3
St. deviation (10 ⁵ Pa)	0.1	0.3	0.4	1.2	0.3	0.6
P ₂ (10 ⁵ Pa)	2.7	2.8	2.8	2.9	3.0	0.9
St. deviation (10 ⁵ Pa)	0.0	0.1	0.1	0.3	1.2	2.1
σ	0.74	0.45	0.28	0.17	0.13	0.03

2.5. Acoustic analysis method

In the frequency range of the study, only acoustic plane waves propagate. The issue is to determine the spectra p^+ and p^- representing, respectively, the upstream and downstream traveling plane waves and for which Fourier-like analysis holds.

From each experiment, time fluctuating-pressure signals are obtained. These data are truncated to a time interval where the acoustic properties do not evolve significantly, i.e. on a duration of about 10 s. With the help of a reference pressure p_{ref} , we compute the cross-spectral densities $G_{pp_{\text{ref}}}(\mathbf{f})$, which are defined as the Fourier Transform of the time correlation (Bendat and Piersol, 1986). It is worth recalling that, for a small frequency bandwidth Δf , the mean-square value of the pressure in the frequency range $[f, f + \Delta f]$ is given by $G_{pp}(\mathbf{f})\Delta f$. These cross-spectra are expressed in Pa^2/Hz . In order to get a spectral expression linear with the pressure, we choose to use the following expression, in $\text{Pa}/\text{Hz}^{1/2}$ (see Appendix A for more details):

$$p_n(\mathbf{f}) = \frac{G_{p_n(t)p_{\text{ref}}(t)}(\mathbf{f})}{\sqrt{G_{p_{\text{ref}}(t)p_{\text{ref}}(t)}(\mathbf{f})}} \quad (1 \leq n \leq 10). \quad (5)$$

For upstream observations, transducer 1 is chosen as reference, and for downstream observations, transducer 10 is chosen as reference.

As plane waves propagate, the acoustic pressure at one point is the summation of the forward (in the direction of the flow) traveling wave p^+ and of the backward traveling wave p^- . We assume the speed of sound to be identical in the forward and in the backward directions, because the Mach number is low (of the order of 10^{-3}). The identification at each transducer of the local speed of sound and of the acoustic plane waves is carried out according to standard intensimetry techniques (Davies et al., 1980; Bodén and Abom, 1986; Hassis, 1999).

The final spectra represent an average of about 20 spectra, determined with a time signal of 10 s duration. Each intermediate spectrum is determined with a window of 1 s duration, and the successive windows have an overlapping ratio of 0.5 (between 0 and 1). This average is made in order to reduce the random errors.

The use of a single reference microphone may give uncertainties for determining standing waves if there is a pressure node at a microphone. This happens when the reflection coefficient is close to unity. At low frequencies (below 500 Hz), this is the case for developed cavitation (see Fig. 6). However, as shown in Fig. 19, the microphones are not close to the pressure nodes of the standing wave patterns. At higher frequencies, and for super cavitation, the reflection coefficient is so low that we do not expect a problem (see Figs. 6 and 7).

2.6. Acoustic boundary conditions on both sides of the orifice

2.6.1. Acoustic boundary conditions upstream of the orifice

The acoustic conditions imposed by the test rig upstream of the orifice are quite reflecting, as illustrated in Fig. 5 by the upstream reflection coefficient $R = p^-/p^+$, defined as the ratio between the forward and the backward propagating plane waves. These reflecting characteristics are due to multiple partial reflections of the acoustic waves on various elements present on the upstream part of the test rig as an open valve, a few bends and section restrictions. Those elements have not been modified in the course of the experiments, so that these reflecting conditions not vary much from one experiment to another.

2.6.2. Acoustic boundary conditions downstream of the orifice

The downstream acoustic boundary condition depends on the cavitation regime, developed cavitation regime or super cavitation regime.

In developed cavitation regime (see Fig. 6), the downstream reflection coefficient has a magnitude close to 1 up to 600 Hz, which indicates a strong reflecting condition. As the phase is a linear function of the frequency, the reflection point is determined: it corresponds to the location of an open valve (at 53D downstream of the orifice). The cavity of this valve is hence filled with a very compressible fluid, i.e. air, imposing an acoustic pressure node $p' = 0$.

The reflection coefficient shows values above unity in Figs. 5 and 6. This may be due to measurement inaccuracies. Also the presence of a noise source outside the main source region is possible and would give values above unity.

In the super cavitation regime (see Fig. 7), the downstream reflection coefficient falls down below the value of 0.5. As a first approximation, the pipe termination is then almost anechoic. This difference of behavior between the developed cavitation regime and the super cavitation regime is not analysed in the framework of the present study.

This variation of the downstream acoustic boundary conditions is specific of the test rig. It has some impact on the levels of the downstream spectra. This will be taken into account further in the study of the downstream noise spectra.

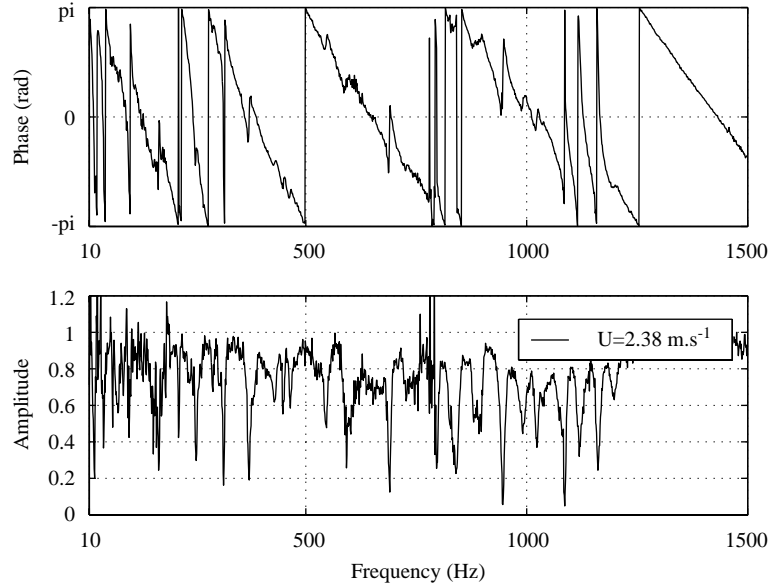


Fig. 5. Typical acoustic reflection coefficient $R = \frac{p^+}{p^-}$ upstream of the orifice (calculated at transducer 1).

It should be pointed out that, for some frequencies, the determination of the acoustical spectra is inaccurate. But coherence values are still good enough, as illustrated in Fig 8, to allow a satisfactory fit of the spectra to determine the speed of sound, as illustrated in Fig. 9.

3. Cavitation regimes

3.1. Hydraulic model for the pressure drop ΔP across the single-hole orifice

A simple model of the hydraulics of the single-hole orifice is proposed. The hydraulic conditions (pressure and Mach number) at the jet of the orifice are estimated, hence giving some insight for a physical interpretation of the different cavitation regimes.

This hydraulic model is a simple classical Borda-Carnot model, see, for example [Durrieu et al. \(2001\)](#). It assumes an incompressible stationary single-phase flow, that is, no effect of cavitation on the hydraulics. Also, the ratio S_j/S between the free jet cross-section and the pipe cross-section S is considered as fixed.

Firstly, mass conservation requires

$$S_j U_j = S U. \quad (6)$$

Secondly, the flow upstream of the jet is assumed to be an inviscid steady potential flow, so that

$$P_1 + \frac{1}{2} \rho_w U^2 = P_j + \frac{1}{2} \rho_w U_j^2. \quad (7)$$

Downstream of the jet, a turbulent mixing region is followed by a uniform flow of velocity U . Neglecting friction at the walls, and assuming a thin ($t/d \lesssim 2$) orifice (with no reattachment of the flow inside the hole of the orifice), one obtains (S_d is the cross-section of the orifice)

$$S P_j + \rho_w U_j^2 S_j = S P_2 + \rho_w U^2 S. \quad (8)$$

The pressure P_j and the velocity U_j at the jet are deduced from Eqs. (6)–(8). The measured pressure drop, denoted by $\Delta P_{\text{measured}}$, is in this case equal to the pressure drop across the orifice: $\Delta P_{\text{measured}} = P_1 - P_2$. Hence, denoting by α the contraction coefficient ($\alpha = S_j/S_d$), this developed cavitation model gives

$$\frac{\Delta P_{\text{measured}}}{(1/2) \rho_w U^2} = \left[\left(\frac{S}{S_j} \right)^2 - 1 \right] + \left[2 - 2 \frac{S}{S_j} \right], \quad (9)$$

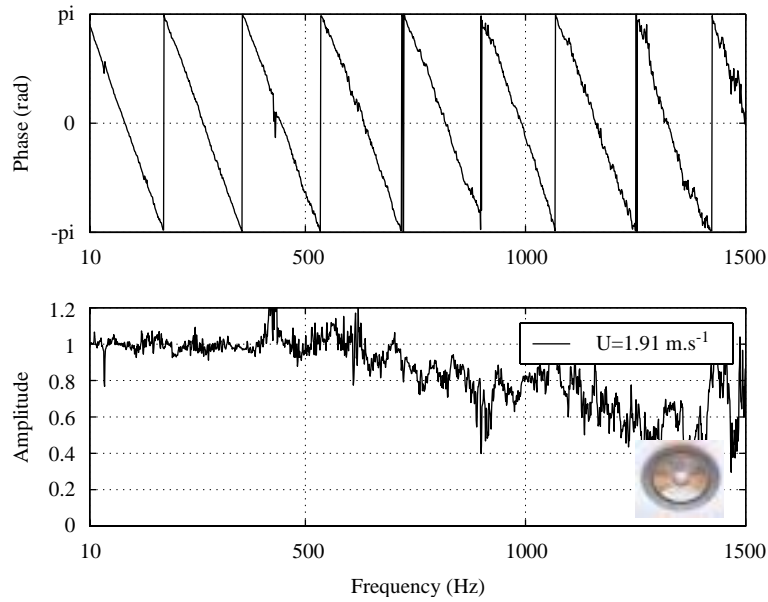


Fig. 6. Typical acoustic reflection coefficient $R = \frac{p_-}{p_+}$ downstream of the orifice (calculated at transducer 8) in developed cavitation regime.

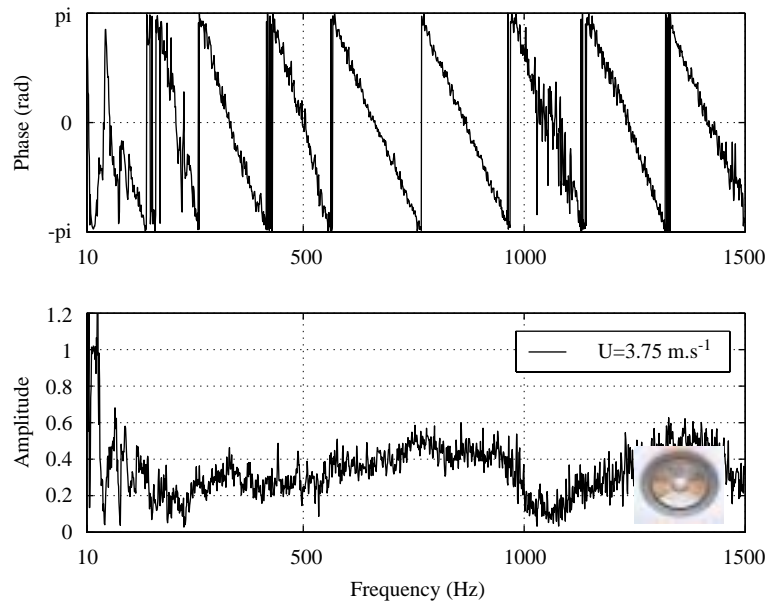


Fig. 7. Typical acoustic reflection coefficient $R = \frac{p_-}{p_+}$ downstream of the orifice (calculated at transducer 8) in super cavitation regime.

the first part representing the dissipation from upstream to the jet, and the second part the dissipation from the jet to downstream.

Finally, after simplifications, we find

$$\frac{\Delta P_{\text{measured}}}{(1/2)\rho_w U^2} = \left[\left(\frac{D}{d} \right)^2 \frac{1}{\alpha} - 1 \right]^2. \quad (10)$$

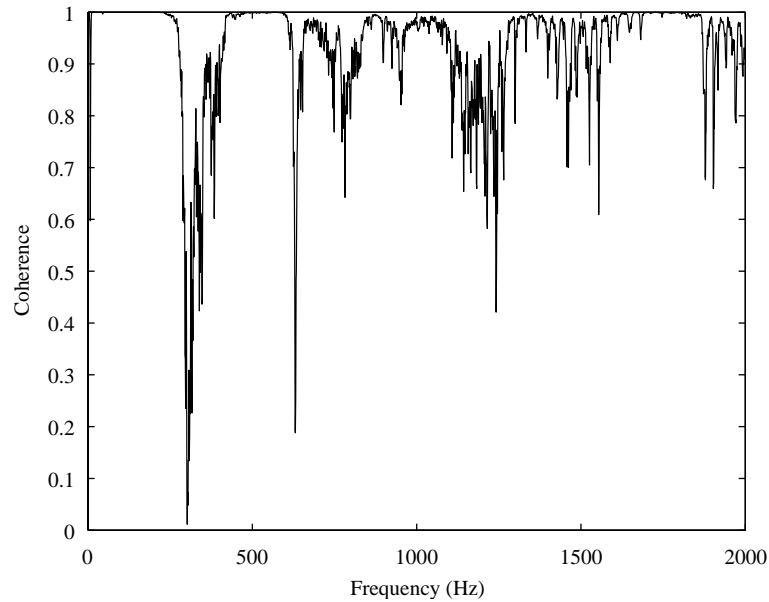


Fig. 8. Example of the coherence function between two successive transducers (single-hole orifice, $U = 2.38 \text{ m s}^{-1}$, between transducers 7 and 8).

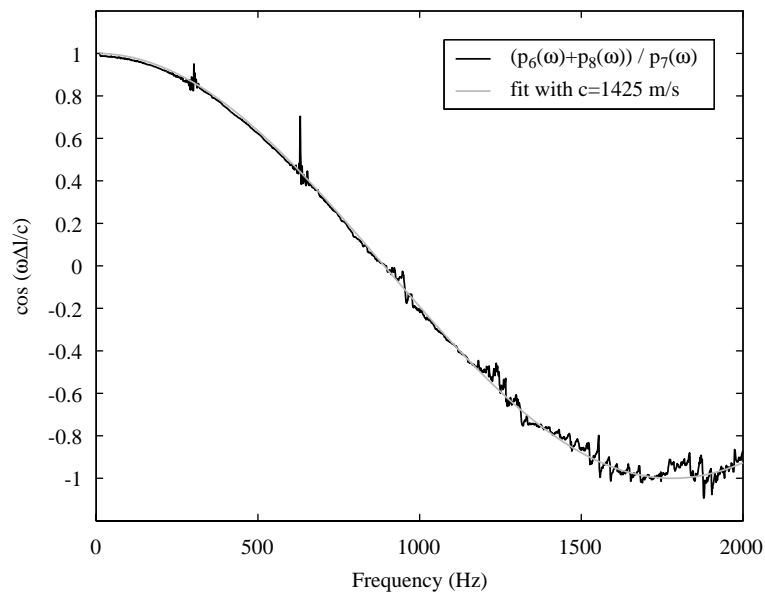


Fig. 9. Example of the determination of the speed of sound using a fit on the spectra for three successive transducers (single-hole orifice, $U = 2.38 \text{ m s}^{-1}$, middle transducer: 7).

In super cavitation, the downstream static sensor is in the jet region, measuring P_j . The pressure drop measured represents the dissipation from upstream to the jet (the first part of the preceding expression):

$$\frac{\Delta P_{\text{measured}}}{(1/2)\rho_w U^2} = \frac{1}{\alpha^2} \left(\frac{D}{d} \right)^4 - 1. \quad (11)$$

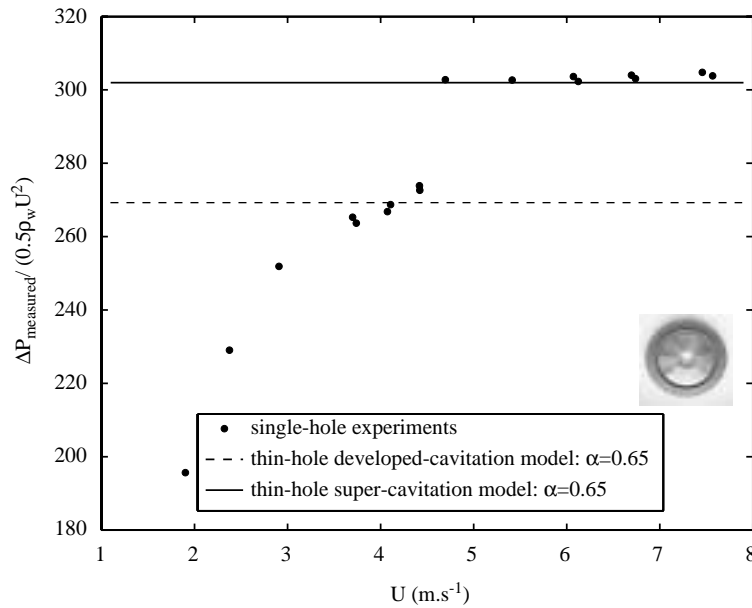


Fig. 10. Comparison between the Borda–Carnot model with different contraction coefficients α and the single-hole orifice measurements.

Table 3
Conditions at the jet using the Borda–Carnot model for the single-hole orifice

	Developed cavitation			Super cavitation				
	U (m s ⁻¹)	U _j (m s ⁻¹)	c _{min} (m s ⁻¹)	P _j (10 ⁵ Pa)	U (m s ⁻¹)	U _j (m s ⁻¹)	c _{min} (m s ⁻¹)	P _j (10 ⁵ Pa)
	1.91	33	28	1.4	3.75	65	13	0.3
	2.38	41	30	1.6	4.08	71	—	—
	2.90	50	34	2.0	4.42	76	—	—

Fig. 10 compares the two models using a contraction coefficient $\alpha = 0.65$ with experimental results (additional experimental results in super cavitation, not shown in Table 1, are plotted), as follows:

- (i) In the developed cavitation regime ($U < 3.5 \text{ m s}^{-1}$), theory agrees qualitatively well with experiments, predicting ΔP within 15%.
- (ii) In the super cavitation regime ($U > 3.5 \text{ m s}^{-1}$), experimental data agree remarkably well with the model, predicting ΔP within 1%. Incidentally, we observe that super cavitation does not induce a strong slope variation in the ΔP versus U curve. This is mentioned in Tullis (1989) for orifices of low d/D ratio (approximately under 0.5, which is the case here).

As a result, the model is validated as a satisfying broad estimation of the hydraulics, taking a contraction coefficient of 0.65. This value is reasonable, as it is close to 0.61 which is the theoretical value for sharp-edged orifices with a jet from a gas to a free space exit (Gilbarg, 1960) and it is less than 0.70, which indicates (Blevins, 1984) that the real radius of curvature of the upstream edge of the orifice is less than 1% of the pipe diameter (this confirms that this edge is a neat sharp angle edge).

Using this model, the pressure and the velocity at the jet are estimated, see Table 3, as follows:

- (a) The pressure in the jet P_j is very close to the vapor pressure of the liquid ($P_v = 5.65 \times 10^3 \text{ Pa}$) in super cavitation regime. This is coherent with the stationary presence of a vapor pocket in this region. Hence, it may be an indicator of the transition to super cavitation regime.
- (b) The velocity U_j is compared to c_{min} , an evaluation of the lowest speed of sound in the two-phase region of the jet. An estimation of it can be obtained, see Van Wijngaarden (1972): the minimum speed of sound is obtained for a

vapor volume fraction in the jet of $\beta = 0.5$, giving $c_{\min} = \sqrt{4\gamma P_j / \rho_w}$. We find (see Table 3) very low values: this is coherent, as there is much vapor in this region. Comparing those values with the velocity of the jet flow U_j , it appears from this crude model that the flow can be ‘supersonic’ in the jet region. This seems relevant in all cavitation regimes, hence this supersonic transition may be characteristic of the transition between a noncavitating and a cavitating flow: it could be an indicator of incipient cavitation. Further research is needed to confirm this idea.

3.2. Hydraulic model for the pressure drop ΔP across the multi-hole orifice

Similarly to the single-hole orifice, a simple model of the hydraulics of the multi-hole orifice is proposed.

Contrary to the single-hole orifice, the multi-hole orifice has a ratio t/d_{eq} over 2 ($t/d_{\text{eq}} = 4.7$), so that each orifice is considered as thick. In that case, for noncavitating flows, there is reattachment of the flow within the orifices, followed by a turbulent mixing region, which corresponds to a first energy loss. A second energy loss is imposed by the sudden enlargement at the exit of the hole.

Following this description, and using similar equations as for the single-hole case, the pressure drop measured across the orifice $\Delta P_{\text{measured}} = P_1 - P_2$ for the developed cavitation regime is composed of a first part representing the dissipation from upstream to the jet (within the orifice), and a second part representing the dissipation after the jet (S_d is the cross-section of the orifice):

$$\frac{\Delta P_{\text{measured}}}{(1/2)\rho_w U^2} = \left[\left(\frac{S}{S_j} \right)^2 - 1 \right] + \left[2 \left(1 - \frac{S}{S_d} \right) + 2 \left(\frac{S}{S_d} \right)^2 \left(1 - \frac{S_d}{S_j} \right) \right]. \quad (12)$$

The total expression is hence the following:

$$\frac{\Delta P_{\text{measured}}}{(1/2)\rho_w U^2} = 1 - 2 \left(\frac{D}{d} \right)^2 + 2 \left(\frac{D}{d} \right)^4 \left(1 - \frac{1}{\alpha} + \frac{1}{2\alpha^2} \right). \quad (13)$$

In the super cavitation regime, we assume that there is no reattachment within the orifice. The downstream static pressure transducer is located intermediately between the two pressure losses, so that the measured pressure loss is given by $\Delta P_{\text{measured}} = P_1 - P_j$. We should again apply Eq. (11) to determine it. As the two orifices have the same open surface, we find the same expression as the developed cavitation model for the single-hole orifice.

Fig. 11 shows comparison of this hydraulic model with experiments, as follows:

- (i) In the developed cavitation regime, the correlation is not good for $\alpha = 0.65$. The pressure drop ΔP is underestimated by about 30%. The thin orifice equation (Eq. (10)), however, performs better, indicating that there is not a full reattachment within the orifice. We observe a reduction of losses for the multi-hole measurements, which is coherent as a two-step dissipation induces less pressure losses than a single step.
- (ii) In the super cavitation regime, the correlation is again excellent, with a prediction of ΔP within 1%.

Conditions at the jet are estimated. We use Eq. (10) with $\alpha = 0.65$ as the most satisfactory for this estimation in developed cavitation. Results are given in Table 4: in the developed cavitation regime, we get the same results as in the single-hole case: the flow is ‘supersonic’ in the sense that the jet flow velocity is higher than the minimum speed of sound in the region; in the super cavitation regime, the estimated pressure at the jet is at the vapor pressure. This also confirms the result obtained for the single-hole case.

3.3. Developed cavitation visualization and temporal signal

In the developed cavitation regime, bubbles are created intermittently, as illustrated in Fig. 12.

The typical time fluctuating pressure signals obtained are difficult to distinguish from a noncavitating flow (see Fig. 13). The fluctuations display a symmetric signal around the mean pressure, with hardly any distinguishable bursts coming from the implosion of the bubbles. Those bursts are discussed later for super cavitation.

3.4. Whistling phenomenon in developed cavitation

Whistling is present in every developed cavitation regime of single-hole orifice experiments (it is never observed for multi-hole orifice experiments). Evidence of whistling is particularly given on the upstream acoustical spectra, by the sharpness of the fundamental frequency peak f_0 and the existence of several harmonics at exact multiples of f_0 (see an

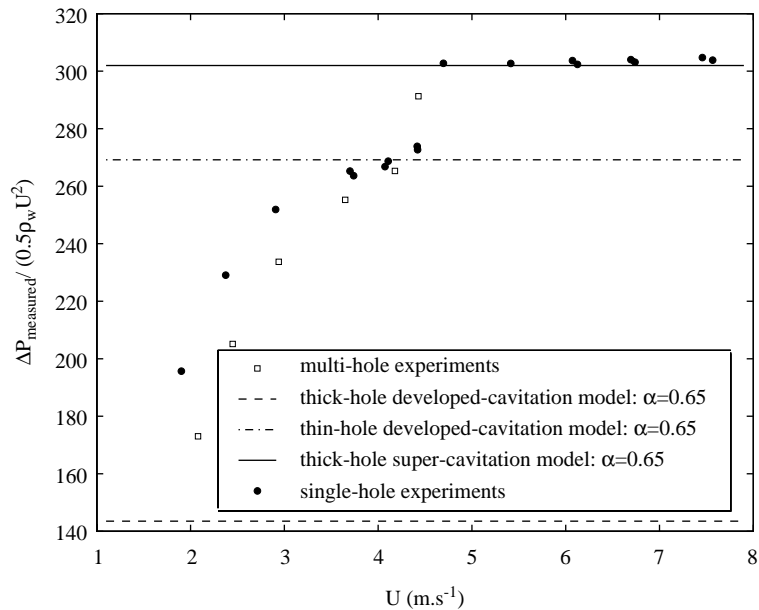


Fig. 11. Evaluation of the multi-hole orifice model and comparison between the single-hole orifice measurements.

Table 4
Conditions at the jet using the Borda–Carnot model for the multi-hole orifice

	Developed cavitation			Super cavitation			
		U (m s ⁻¹)	2.08	2.45	2.94	3.65	4.18
	U _j (m s ⁻¹)	36	43	51	63	73	77
	c _{min} (m s ⁻¹)	20	—	27	—	—	—
	P _j (10 ⁵ Pa)	0.7	—	1.3	—	—	—

example in Fig. 14). The higher harmonics are typical of steady whistling stabilized by a nonlinear feedback effect as for all self-sustained oscillations (Fletcher, 1979; Rockwell and Naudascher, 1979).

Scant literature has been found on whistling of cavitating orifices in pipes. A vortex shedding phenomenon in presence of cavitation has been investigated by Sato and Saito (2001), but in the particular case of thick orifices ($t/d \gtrsim 2$). On thin orifices, some visualizations (Moussou et al., 2003) made on other EDF experiments have shown the possibility of the presence of vortex-shedding in cavitation regime, as can be seen in Fig. 15, from Archer et al. (2002).

The whistling frequencies are given in Table 5. They do not increase continuously with the flow velocity, as one would expect for a hydrodynamic oscillation edge-tone like (Blake and Powell, 1983). The stable frequency is typical of an acoustic feedback which creates and maintains the acoustic oscillation close to a resonance frequency. This is also revealed by the locking of the phase of the time pressure signals on successive sensors, which indicates a standing wave pattern.

Upstream of the orifice, the level of whistling is higher than downstream: hence the acoustic feedback is suspected to happen predominantly upstream. The upstream reflection coefficient, see Fig. 5, is reflecting but irregular: no clear acoustic reflection point can be identified (as it can be for the cavity of a valve downstream, see Section 2.6.2). This irregular shape is due to the intricacy of the upstream rig design, with a succession of elbows, slight restrictions of sections and some open valves.

It is also worth mentioning that the whistling frequency does not coincide with any downstream natural acoustic frequency. This is coherent with the acoustic uncoupling observed from both sides of the orifice.

The single-hole orifice has a ratio $t/d = 0.6$, inferior to 2, so that it is considered as a thin orifice. We assume that the whistling phenomenon is influenced by the thickness of the orifice t , rather than its diameter. It is also natural to use the

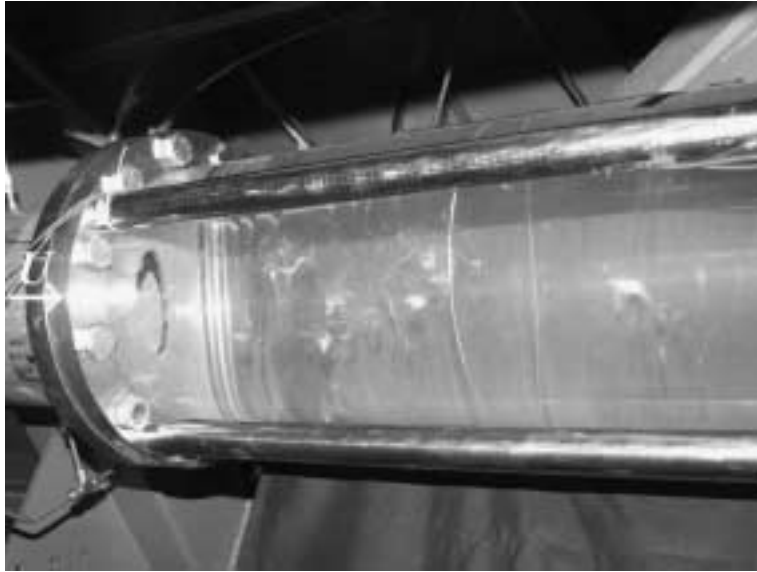


Fig. 12. From other experiments at EDF (Archer et al., 2002), visualization of the developed cavitation regime for a single-hole orifice ($d/D = 0.30$, $t/d = 0.10$, $D = 2.66 \times 10^{-1}$ m) with $\sigma = 0.49$ and $U = 1.50 \text{ m s}^{-1}$ ($\Delta P = 3.1 \times 10^5$ Pa, $P_1 = 4.6 \times 10^5$ Pa). White bubble clouds are observed around the jet formed at the orifice.

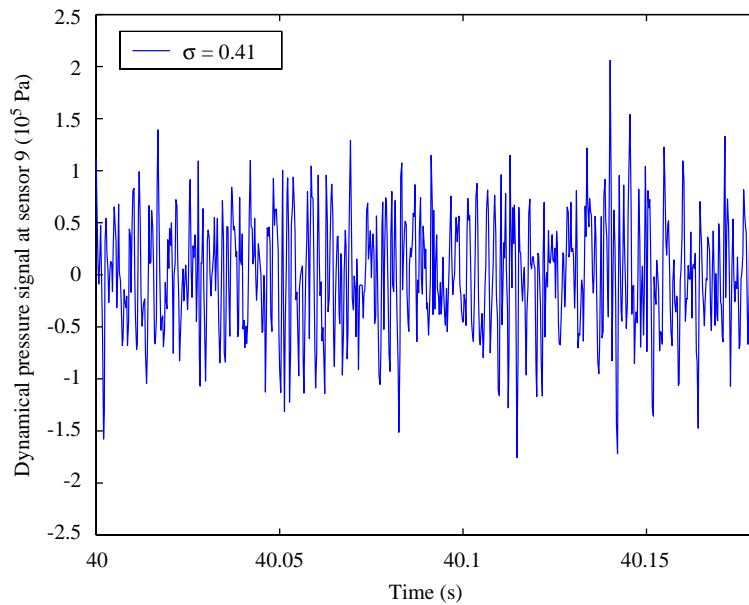


Fig. 13. Typical dynamical time pressure signal from a downstream transducer for the developed cavitation regime (here for the single-hole orifice at $\sigma = 0.41$).

velocity at the orifice U_d as a relevant scaling velocity. Hence the Strouhal number is defined as

$$St = \frac{f_0 t}{U_d}, \quad (14)$$

and values are reported in Table 5.

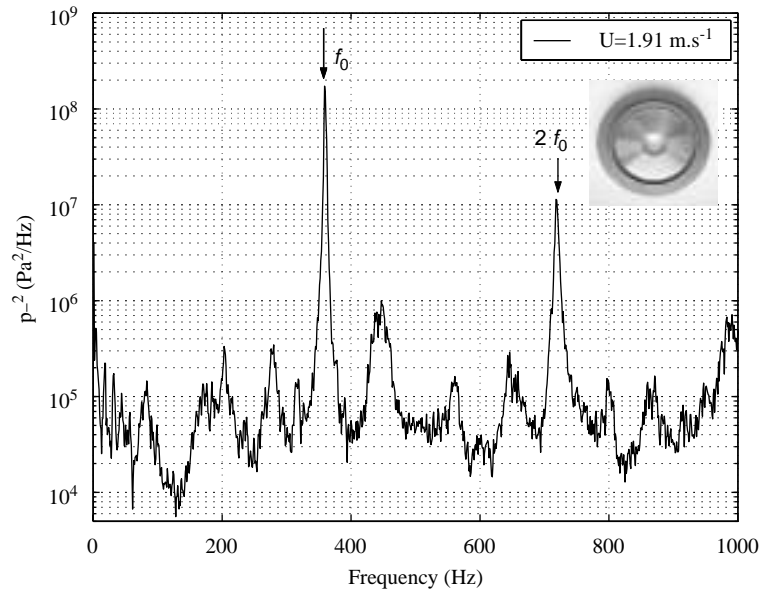


Fig. 14. Detection of whistling frequency f_0 with harmonics on upstream plane wave spectra p^- (here for the single-hole orifice at $U = 1.91 \text{ m s}^{-1}$, $f_0 = 359 \text{ Hz}$ and the first harmonics at 718 Hz).



Fig. 15. From other experiments at EDF (Archer et al., 2002), visualization of a cavitating and whistling single-hole orifice ($d/D = 0.30$, $t/d = 0.10$, $D = 2.6 \times 10^{-1} \text{ m}$) with $\sigma = 0.35$ and $U = 1.97 \text{ m s}^{-1}$ ($\Delta P = 5.3 \times 10^5 \text{ Pa}$, $P_1 = 7.2 \times 10^5 \text{ Pa}$).

The Strouhal number is obtained in the range 0.18–0.26. These values are close to data on orifices: Anderson (1953) finds a Strouhal number around 0.2 for whistling orifices in air with a free air exit. In Anderson's experiments, the orifices were a bit thinner (with $0.2 \leq t/D \leq 0.5$, whereas here $t/D = 0.19$) and the Reynolds numbers smaller ($U_d t / \nu_{\text{air}} \sim 10^3$ with ν_{air} the kinematic viscosity of air, whereas here $U_d t / \nu_{\text{water}} \sim 10^5$).

The multi-hole orifice is a thick one, as $t/d_{\text{multi}} = 4.7$. Hence it is no surprise that it does not whistle. The flow reattaches itself inside each hole, which stabilizes the shear layers of the jet and hence prevents whistling in the same manner as observed for the single-hole orifice.

Table 5

Strouhal number $St = f_0 t / U_d$ of the whistling frequency f_0 (only observed in the single-hole orifice case)

	U (m s^{-1})	1.91	1.91	2.38	2.38	2.90	2.90
	c (m s^{-1})	1390	1200	660	1420	1130	1420
	f_0 (Hz)	359	397	421	436	427	434
	St	0.23	0.26	0.22	0.23	0.18	0.19



Fig. 16. From other experiments at EDF, visualization of the super cavitation regime for a single-hole orifice.

3.5. Super cavitation visualization and typical temporal signal

In the super cavitation regime, a vapor pocket is created in the jet region, as illustrated in Fig. 16.

When the vapor pocket expands and reaches the downstream transducers, those transducers no longer deliver any acoustical signal. This constitutes an evidence for the existence of the vapor pocket.

It appears that the length of the vapor pocket increases quickly with flow velocity. The length of the vapor pocket increases from about $7D$ at $U_0 = 3.8 \text{ m s}^{-1}$ to $18D$ at $U_0 = 4.4 \text{ m s}^{-1}$ and is larger than $38D$ at $U_0 = 4.7 \text{ m s}^{-1}$ for the single-hole orifice. For the multi-hole orifice, the length of the vapor pocket increases from around $7D$ at $U_0 = 4.2 \text{ m s}^{-1}$ to larger than $38D$ at $U_0 = 4.5 \text{ m s}^{-1}$.

The typical time-fluctuating pressure signals obtained are very different from those in the developed cavitation regime (see Fig. 17). They are asymmetric around the mean pressure, exhibiting very large positive spikes, up to 20 bar, linked to the collapse of bubbles.

Focusing on time signals (see an illustration in Fig. 18), it is seen that the phenomenon of bubble implosion is characterized first by a decrease in negative values of the fluctuating pressure with a characteristic duration of a tens of milliseconds, followed by an abrupt increase of the pressure, a ‘spike’, with a characteristic duration of 1 ms. By modeling this bubble volume evolution with a monopole source, which is a common and satisfactory simple model; see, for instance, Brennen (1995), the first decrease is linked with a decrease of the bubble size from its initial size to a value close to zero; the second part of the signal is linked with a pressure shock wave originating from the abrupt collision of the water particles. However, extremely high amplitudes are observed in comparison to Brennen (1995) (cf. Fig. 3.19). This can be due either to the large size of our bubbles or to the effect of confinement.

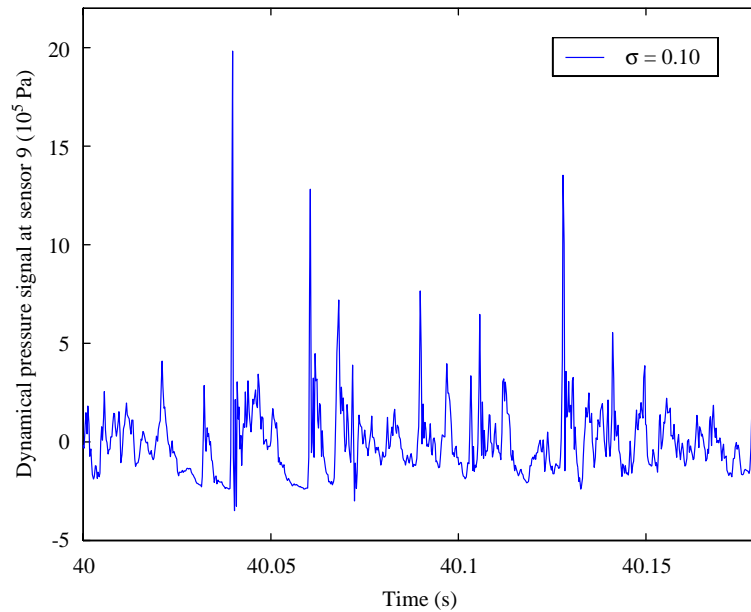


Fig. 17. Spurious pressure pulses (spikes) from collapsing bubbles on dynamical time pressure signal from a downstream transducer in super cavitation regime (here for the single-hole orifice at $\sigma = 0.10$).

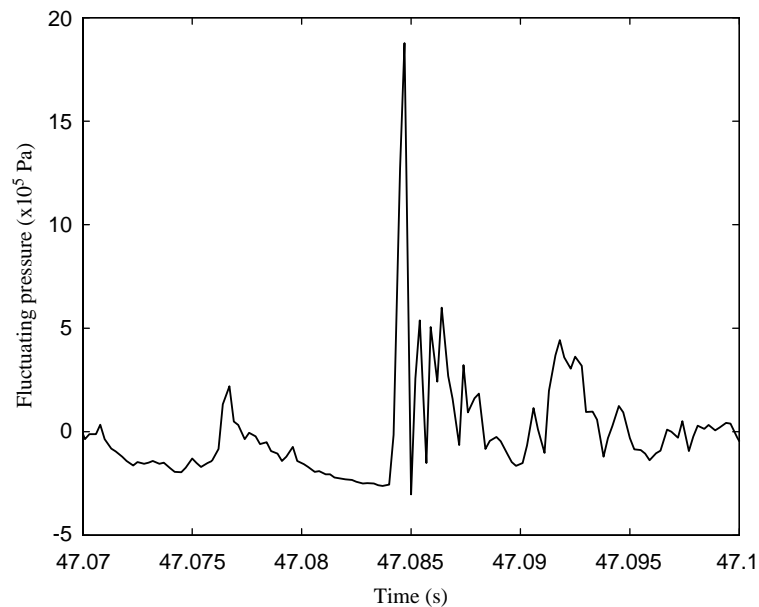


Fig. 18. Cavitation peak in super cavitation regime (single-hole orifice at $\sigma = 0.10$).

4. Results in the developed cavitation regime

The single-hole and the multi-hole orifice developed cavitation regimes are presented together, as they show similar acoustical behavior. Firstly, results on the acoustic features of this cavitation regime are introduced: the observed variations of the downstream speed of sound and the presence of resonance frequencies in downstream spectra. Then the downstream spectra, depending on those acoustical features, are presented and discussed.

4.1. Acoustic features

4.1.1. Spontaneous variations of the downstream speed of sound

For a fixed set of hydraulic conditions in the developed cavitation regime, the downstream speed of sound may spontaneously evolve. For instance, the single-hole orifice experiment at $U = 2.38 \text{ m s}^{-1}$ shows the downstream speed of sound evolving from 660 m s^{-1} (during the first 20 s) to 1420 m s^{-1} (till the end of the experiment: 90 s).

This variation of the speed of sound indicates that air bubbles are present, in varying quantity, in the water far downstream of the orifice. For instance, a value of 660 m s^{-1} indicates a volume gas fraction in the water between 10^{-3} and 10^{-4} , assuming the static pressure being between P_1 and P_2 [we use a classic formula; see, for example, Van Wijngaarden (1972)]. On the contrary, a value of 1420 m s^{-1} indicates a negligible content of air in the water, as it is close to the speed of sound in pure water [which equals to 1454 m s^{-1} , as presented in Section 2.3.1].

Cavitation bubbles, when they are formed, are originally mainly constituted of vapor. During their lifetime, they are gradually filled with air, due to the diffusion of the dissolved gas present in the water surrounding them. As they drift downstream, moving away from their region of creation, they reach regions where the pressure recovers higher levels. Pure vapor bubbles cannot persist, those bubbles remaining far downstream of the orifice are mainly filled with air (see for example Fig. 12). Consequently, the observed variation of the quantity of air bubbles is suspected to be due to an inhomogeneity of the dissolved gas content in the injected water. This inhomogeneity may be related to temperature variations in the experimental installations. This hypothesis is all the more plausible as the water used has not received any degassing treatment, hence having a fluctuating and high dissolved gas content, not measured but estimated around 10^{-2} or 10^{-3} (values at saturation conditions for $T = 273$ and 310 K , respectively). In some experiments, the change in residual air bubble content occurs after the water from the pipe segment between the orifice and the tank has been evacuated and 'fresh' tank water has started to flow through the orifice.

These variations of the downstream speed of sound during each experiment have some influence on the acoustical behavior downstream of the orifice: the values of the natural frequencies, appearing downstream, are altered proportionally with the speed of sound.

The propagating waves are subjected to two-phase flow damping, as already mentioned by Hassis (1999). As regards this last effect, no significant variation of the propagating wave amplitude could be measured along the downstream sensors, but the downstream acoustical reflection coefficient appears to vary significantly with the downstream speed of sound.

4.1.2. Acoustical uncoupling from both sides of the orifice

An acoustical uncoupling is observed between acoustical spectra upstream and downstream of the orifice: the natural frequencies present downstream are strongly attenuated on upstream spectra; the whistling, when present, is visible on upstream spectra, but hardly on downstream spectra; and, furthermore, the background noise on downstream spectra is higher than the one on upstream spectra, approximately from a factor 2 (for $U = 1.91 \text{ m s}^{-1}$) up to 7 (for $U = 2.90 \text{ m s}^{-1}$) for the single-hole orifice, and much more significantly for the multi-hole orifice, with an approximately constant factor of about 10.

This acoustical uncoupling is an effect of cavitation as there is choking (indicated in Table 3).

4.1.3. Presence of natural modes downstream

In this developed cavitation regime, resonance frequencies are systematically observed in acoustical spectra downstream of the orifice (both for the single-hole and the multi-hole).

The acoustic boundary conditions are of a similar type, as the frequencies are of the form: $f_n = n f_1$, f_1 being the first resonance frequency. More precisely, these acoustic boundary conditions can be identified by extrapolating the standing wave patterns at those resonance frequencies. This extrapolation is made possible as a series of transducers (7 in number) is present downstream of the orifice. As a result, we find two acoustic pressure nodes $p' = 0$ (see Fig. 19), discussed above, as follows:

- (i) One acoustic pressure node is found far downstream of the orifice, at $52D (\pm 1D)$. It is the result of the influence of a cavity of an open valve filled with air. The reflection coefficient imposed by such a cavity has been presented in Fig. 6. The magnitude of the reflection coefficient $|R|$ is close to 1, which confirms the acoustic influence of this cavity.
- (ii) Another is found just downstream of the orifice, at $4D (\pm 1D)$. It is likely to be caused by a cavitation cloud.

4.2. Noise spectra generated downstream

Noise spectra generated in the pipe downstream of the orifice for the developed cavitation regime are presented in this section.

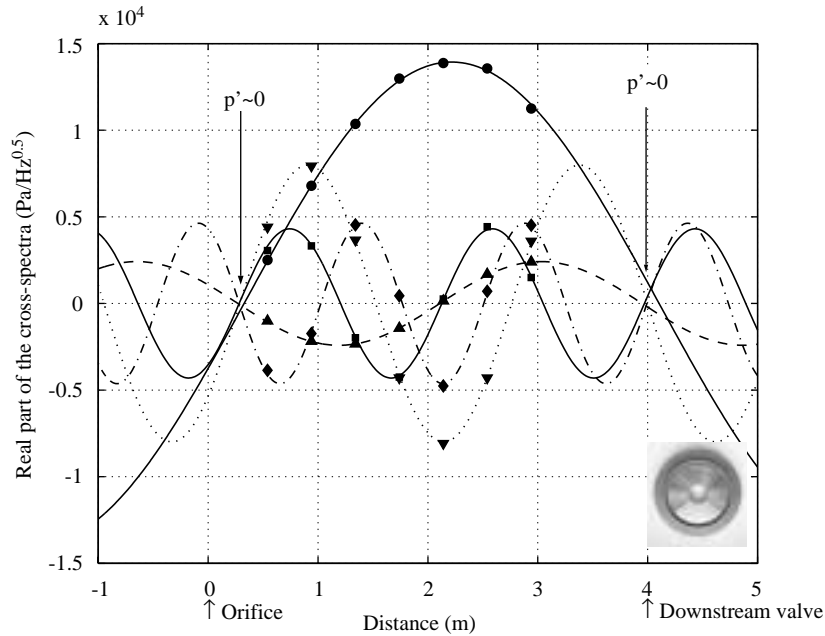


Fig. 19. In the developed cavitation regime, two acoustic boundary conditions $p' \simeq 0$ are found downstream of the orifice, hence natural frequencies appear, pointed out by the interpolation of the values of the cross-spectra at those first natural frequencies (here for the single-hole orifice at $U = 2.38 \text{ m s}^{-1}$, $c = 1420 \text{ m s}^{-1}$ and five natural frequencies: ● 188 Hz, ▲ 386 Hz, ▼ 574 Hz, ■ 770 Hz, ◆ 957 Hz).

The downstream transducers give a far-field measurement, as they are not located in the source region mainly constituted of bubble implosions located just downstream of the orifice. The acoustical power measured at downstream transducers represents the noise generated in the pipe. Under the assumptions of plane-wave propagation and no influence of the flow (the Mach number is around 10^{-3}), the acoustical power takes the expression: $S(p^{+2} - p^{-2})/(\rho_w c_w)$ (Morfey, 1971).

It is furthermore assumed that the backward propagating wave spectrum of p^- is small enough to be neglected. Even if acoustical reflection is observed to occur downstream, this estimation of the source of noise is considered satisfactory enough as an order of magnitude (this is all the more relevant as logarithmic representation is used). Thus, it comes to the source power being represented by the quantity $S p^{+2}/(\rho_w c_w)$.

Of course, this representation is no more valid for the discrete frequencies which are whistling harmonics and resonance frequencies, as the backward propagating wave has great influence in those cases.

The acoustical power spectra obtained downstream of the orifice for the developed cavitation regime are given in Fig. 20 for the single-hole orifice and in Fig. 21 for the multi-hole orifice. The rejection frequency corresponding to a wavelength of half of the distance between two successive transducers and depending on the measured speed of sound has been excluded from those results. The following observations are made on those spectra:

- spectra exhibit a hump form in the upper frequency range (above 200 Hz); this hump form is typical of cavitation noise (Martin et al., 1981; Brennen, 1995);
- the single-hole orifice generates remarkably much more noise (by a factor of about 10^2 in the acoustical power) than the multi-hole orifice.

4.3. Nondimensional analysis and representation

4.3.1. Choice of the scaling variables for the noise spectra

Scaling is proposed in order to obtain a dimensionless representation of the acoustical source power.

Cavitation noise from the implosions of bubbles is assumed to be predominant in order to scale the noise spectra. Hence, broadband turbulence noise from the mixing region downstream, whistling and resonance frequencies are not

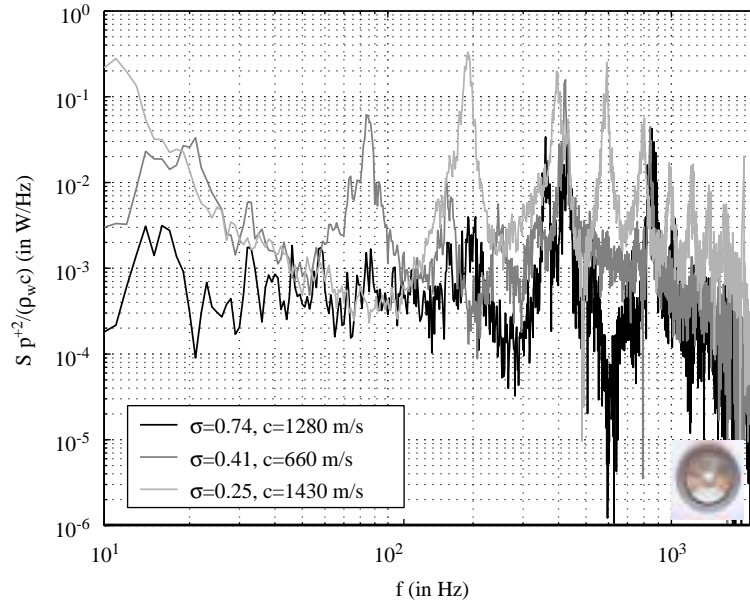


Fig. 20. Acoustical power spectra in developed cavitation (single-hole orifice).

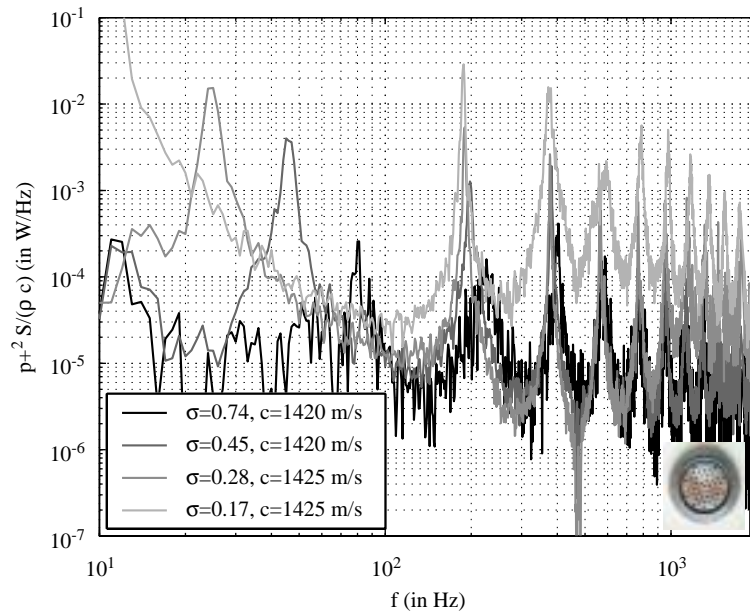


Fig. 21. Acoustical power spectra in developed cavitation (multi-hole orifice).

taken into account to choose the scaling variables. This assumption of predominance of cavitation noise is globally valid, but seems to fail at low frequencies (in this work, below 200–300 Hz approximately). Also, it is assumed that whistling does not alter cavitation noise, generalizing the hypothesis that broadband noise is not affected by whistling [as shown in [Verge \(1995\)](#) for a flue organ pipe].

Following [Blake \(1986\)](#), the amplitude of noise produced by cavitation should be made dimensionless by dividing with the downstream pressure, and not the pressure drop, when using a Rayleigh–Plesset bubble dynamic model for a spherical isolated free bubble. However, ring vortices generated by an orifice are not isolated bubbles in free space, so

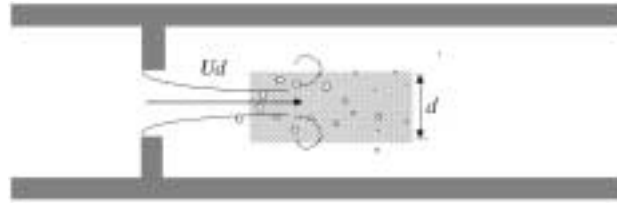


Fig. 22. Choice of the variables d and U_d for the scaling of the noise spectra in the developed cavitation regime for the single-hole orifice.

that this scaling should not hold in the case of the present study, as it also does not for sheet cavitation on airfoils (Keller, 1994).

As we lack a precise model, the scaling data are chosen for the sake of simplicity: the basic idea, as shown in Fig. 22, relies on the fact that, in the developed cavitation regime, the bubbles are created in the mixing high-shear region of the jet.

For the single-hole orifice experiments, the velocity U_d and the orifice diameter d are representative of the conditions in this region, hence those quantities are used in order to scale the noise spectra in this regime. Furthermore, the scaling pressure is defined as the pressure drop ΔP across the orifice, which is a measure of the kinetic energy density in the jet. Hence for the single-hole orifice in developed cavitation, fd/U_d is the nondimensional frequency and $p^{+2}U_d/(\Delta P^2d)$ is the nondimensional magnitude.

For the multi-hole orifice experiments, we assume the noise issuing from incoherent N_{holes} sources.

Each source represents the radiation of one hole. It radiates on a characteristic surface of S/N_{holes} . The strength of each source is assumed to be independent of the environment of the source. This assumption is natural, as we have previously supposed (see previous section) that the noise generated by the single-hole orifice does not depend on the diameter of the pipe. However, it should be pointed out that this assumption is wrong when whistling occurs.

In this model, the total acoustic power P measured downstream is a summation of the acoustic power $P_{\text{each source}}$ emitted by each source [the key element is that sources are supposed to be incoherent between each other, see Pierce (1981)]:

$$P = N_{\text{holes}}P_{\text{each source}}. \quad (15)$$

The acoustic power of each source $P_{\text{each source}}$ is, by definition, the total acoustic intensity flux I multiplied the surface of this source:

$$P_{\text{each source}} = IS/N_{\text{holes}}. \quad (16)$$

Hence the total acoustic power is

$$P = SI. \quad (17)$$

The total acoustic power is consequently independent of the number of holes. As previously, we ignore any downstream reflections, so that $I = p^{+2}/(\rho c)$.

This argumentation based on energy considerations can also be conducted in terms of forces: if the source is represented as a force acting on the orifice, taking the form Sp^+ , the total force imposed on the multi-hole orifice is due to the contribution of the forces imposed by N_{holes} equivalent single-hole orifices with open surface S/N_{holes} . Those forces are supposed to be uncorrelated with each other. Thus, the total force squared equals N_{holes} times the force squared due to one hole. As the force squared of one hole is $(p^+S/N_{\text{holes}})^2$, the total force squared is expressed as: $N_{\text{holes}}(p^+S/N_{\text{holes}})^2$, or by simplifying: $(p^+S)^2/N_{\text{holes}}$.

The scaling of the acoustic power is based on each source of surface S/N_{holes} . The scaling velocity is the velocity at the orifice, which is taken equal to the velocity of the single-hole orifice U_d , as the open surface of the two orifices are very similar, and the scaling length is the diameter of one hole d_{multi} . In conclusion for the multi-hole orifice in developed cavitation: fd_{multi}/U_d is the nondimensional frequency, and $p^{+2}U_d/(\Delta P^2d_{\text{multi}})$ is the nondimensional magnitude.

4.3.2. Nondimensional noise spectra generated downstream

The dimensionless acoustical power spectra obtained downstream of the orifice for the developed cavitation regime are given in Fig. 23 for the single-hole orifice and in Fig. 24 for the multi-hole orifice. The following observations are worth noting.

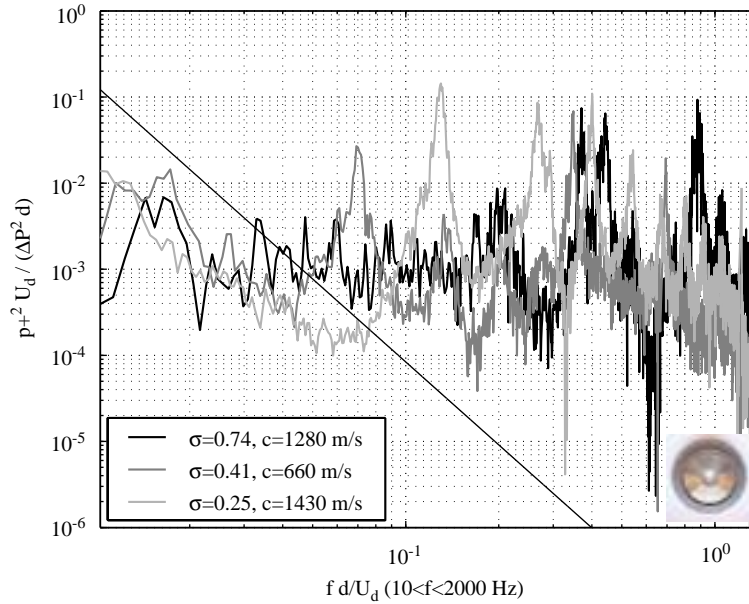


Fig. 23. Nondimensional acoustical power spectra in developed cavitation (single-hole orifice). Straight line: dimensionless turbulence level estimation of Moussou (2005).

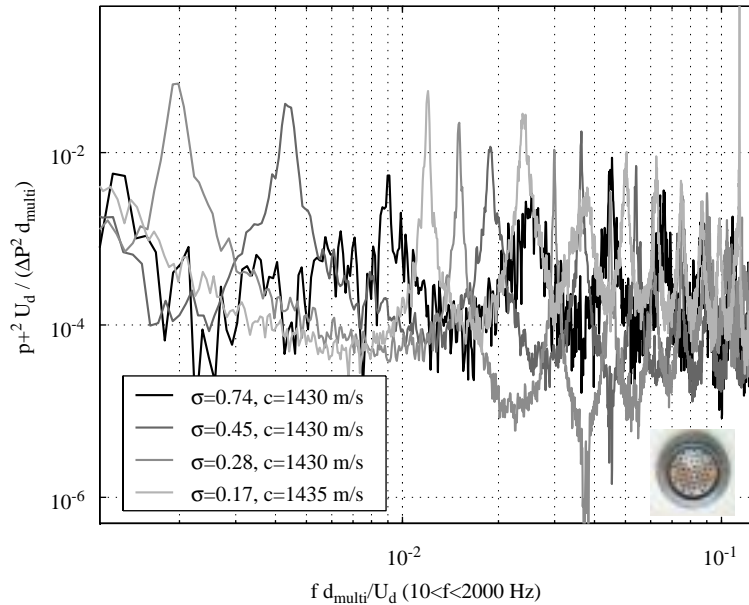


Fig. 24. Non-dimensional acoustical power spectra in developed cavitation (multi-hole orifice).

(a) The scaling for the single-hole orifice and the multi-hole orifice is efficient as the nondimensional noise spectra collapse for each orifice. This is illustrated in Fig. 23 for the single-hole orifice and Fig. 24 for the multi-hole orifice. Hence it is found that these spectra do not depend significantly on the cavitation number or on the downstream speed of sound. However, the dispersion of the scaling variables is weak, so that additional data should be added to confirm this result.

- (b) The different scaling used for the single-hole and the multi-hole orifice is rather efficient as it makes the levels of the two types of orifices closer to each other. However, the nondimensional level of noise of the single-hole orifice is still higher, with a ratio of 10, than the one of the multi-hole orifice experiments; see Figs. 23 and 24.
- (c) We compare the cavitation noise with a standard turbulence noise from a noncavitating orifice in the low frequency range. Indeed, in this range of frequency, the level of noise is expected to be mainly determined by turbulence noise (Martin et al., 1981). We use a nondimensional turbulence noise level proposed by Moussou (2005). In this model, the scaling is based on empirical data obtained with simple singularities (single-hole orifice, valve) in water-pipe flow: the level of noise is assumed to depend only on a Strouhal number based on the pipe diameter and the pipe flow velocity. We apply this model with the values of the pipe diameter D and a pipe flow velocity of 2.20 m s^{-1} and compare it to the single-hole orifice nondimensional noise, see Fig. 23. As expected, the turbulence level fits rather well the cavitation noise at low frequencies, with a good estimation of the slope; the cavitation noise is much stronger than the turbulence noise above the low-frequency range, which is a well-known result Brennen (1995).

5. Results in the super cavitation regime

5.1. Acoustic features

The super cavitation experiments exhibit two main differences compared to the developed cavitation experiments, as follows:

- (i) The downstream speed of sound appears to be quite constant during each experiment.
- (ii) No resonance frequencies are found on downstream spectra. The downstream reflection coefficient is much lower than in the developed cavitation case (as previously shown in Fig. 7). In this case, the cavity of the downstream valve does not reflect the acoustic waves.

As for the developed cavitation case, strong acoustic uncoupling is observed from both sides of the orifice. The effect is much more obvious here, with an average ratio between downstream and upstream power spectra of about 2–30 for the single-hole orifice case, and about 10–50 for the multi-hole orifice case.

5.2. Noise spectra generated downstream

Noise spectra obtained downstream are given in Fig. 25 for the single-hole orifice and in Fig. 26 for the multi-hole orifice (as previously, the rejection frequencies being excluded). We note the following points:

- (i) The typical cavitation hump form is observed, as in the developed cavitation case, but with much more evidence. The level of the hump is higher than for the developed cavitation regime; also, the frequency peak is smaller: those tendencies when the cavitation number increases confirm literature data Brennen (1995).
- (ii) Also, as in the developed cavitation case, the single-hole orifice is clearly more noisy (with an approximate factor of 10 on acoustical power spectra) than the multi-hole orifice.

An important result is illustrated in Figs. 26 and 27: the part of the spectra succeeding the hump peak frequency depend strongly on the downstream speed of sound. Two-phase flow attenuations phenomena are supposed to be the cause of this observation.

6. Conclusion

A single-hole and a multi-hole cavitating orifice in a water pipe have been studied experimentally under industrial conditions, i.e. with a pressure drop varying from 3 to 30 bar and a cavitation number in the range $0.03 \leq \sigma \leq 0.74$.

In the regime of developed cavitation, whistling is observed for the single-hole orifice. This occurs at a Strouhal number based on the orifice thickness with a value close to 0.2.

Our results indicate that in the developed cavitation regime, a multi-hole orifice is much more silent than a single-hole orifice with the same total cross-sectional opening. This might be partially explained by the absence of correlation

between the sound produced by different holes in the absence of whistling. No such difference is found in super cavitation. This is explained by the fact that, in the super cavitation regime, sound is produced far downstream of the orifice rather than in a near region downstream of the orifice.

A nondimensional noise source is proposed for the developed cavitation regime (cf. Section 4.3). The source model seems satisfactory for the developed cavitation case.

The results presented are certainly limited and call for further research. In particular, it could be interesting to vary the shape of the orifices and repeat the experiments with degassed water.

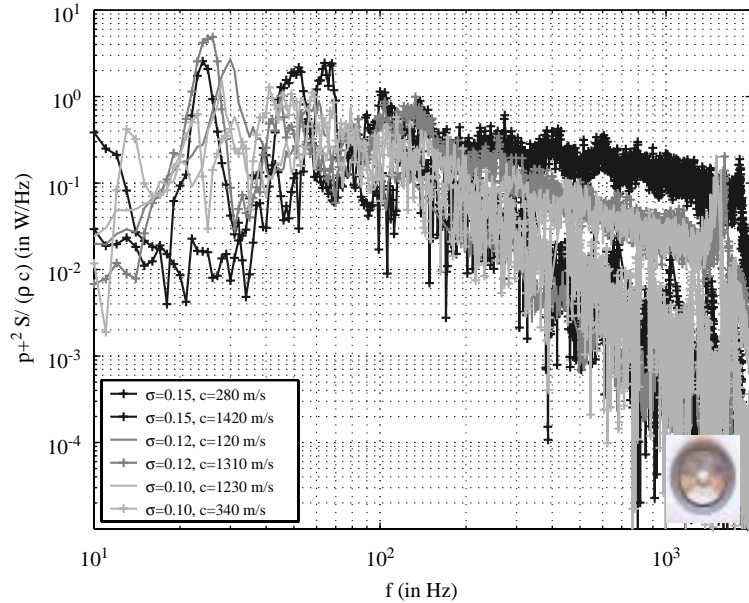


Fig. 25. Acoustical power spectra in super cavitation (single-hole orifice).

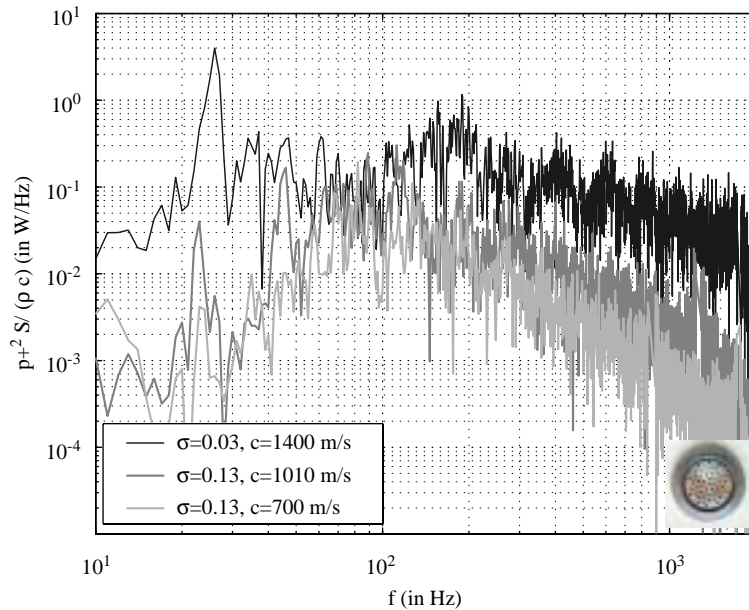


Fig. 26. Acoustical power spectra in super cavitation (multi-hole orifice).

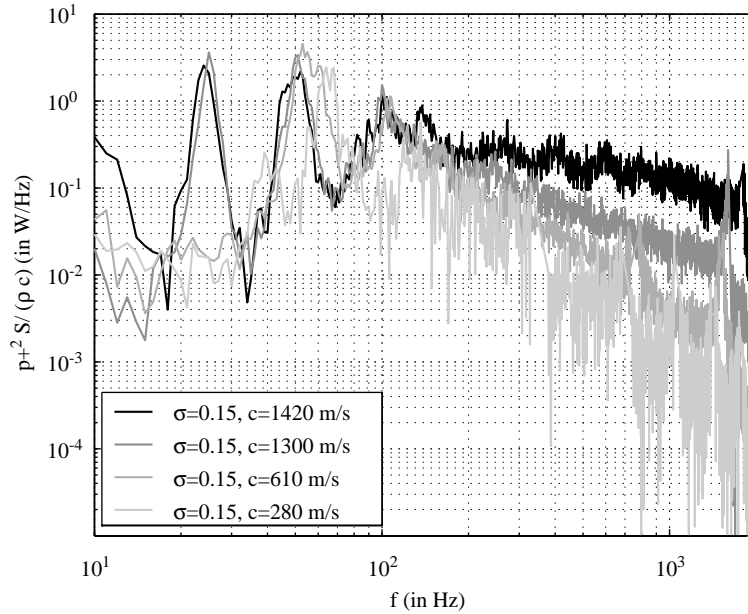


Fig. 27. Super cavitation (single-hole orifice): influence of the speed of sound on the noise spectra.

Acknowledgment

The experiments have been designed and realized by MM. S. Caillaud, Ch. Martin and L. Paulhiac.

Appendix A. Acoustic analysis

We assume that only plane waves propagate in the pipe. First, cross-spectral density functions $G_{pp_{ref}}$ are used. They are well suited to acoustic analysis, because they eliminate nonpropagating noise present in time measurements. Indeed, if we decompose time pressure measurements $p(t)$ into a nonpropagating signal $p^{nonprop}(t)$ and a propagating one, we have

$$p(t) = p^+(t) + p^-(t) + p^{nonprop}(t). \quad (A.1)$$

Having defined and fixed a reference sensor and applying the cross-spectral density functions, we get an expression where the nonpropagating pressure is removed because it is not correlated to the propagating pressure:

$$G_{p(t)p_{ref}(t)}(\omega) = G_{p^+(t)p_{ref}(t)}(\omega) + G_{p^-(t)p_{ref}(t)}(\omega). \quad (A.2)$$

Second, we define quantities $G_{pp_{ref}}/\sqrt{G_{p_{ref}p_{ref}}}$ which can be handled like Fourier Transforms, and which are almost independent of the reference pressure. Indeed, if we assume a perfect coherence between the point of observation and the reference sensor, we have

$$\frac{|G_{pp_{ref}}|^2}{G_{pp} G_{p_{ref}p_{ref}}} = 1. \quad (A.3)$$

In this case the quantity $G_{pp_{ref}}/\sqrt{G_{p_{ref}p_{ref}}}$ does not depend on the reference sensor. In practice, the reference sensor is taken closest to the points of observation.

Finally, we calculate plane waves. Considering two consecutive sensors, denoted n and $n+1$, plane waves propagation and the linearity characteristics of the cross-spectral density function give

$$G_{p_{n+1}^+ p_{ref}}(\omega) = G_{p_n^+ p_{ref}}(\omega) e^{-j\omega\tau}, \quad (A.4)$$

$$G_{p_{n+1}^- p_{ref}}(\omega) = G_{p_n^- p_{ref}}(\omega) e^{+j\omega\tau}, \quad (A.5)$$

with τ being the time of flight of the wave between the two sensors. For the sake of ease, we note p_n for $G_{p_n \text{ Pref}} / \sqrt{G_{p_n \text{ Pref}}}$. By means of Eqs. (A.2), (A.4) and (A.5), we get the plane wave spectra:

$$p_n^+(\omega) = \frac{p_n(\omega) e^{+j\omega\tau} + p_{n+1}(\omega)}{2j \sin(\omega\tau)}, \quad (\text{A.6})$$

$$p_n^-(\omega) = \frac{p_n(\omega) e^{-j\omega\tau} + p_{n+1}(\omega)}{-2j \sin(\omega\tau)}, \quad (\text{A.7})$$

for upstream measurements ($1 \leq n \leq 2$) and downstream measurements ($4 \leq n \leq 9$). These spectra are expressed in $\text{Pa}/\sqrt{\text{Hz}}$.

The reflection coefficient is defined as p^-/p^+ downstream of the orifice, and by p^+/p^- upstream, because we assume the source of sound to be located in the region of the orifice. For example, if a zero pressure condition is located far downstream of the orifice, and if T is the time of flight toward this pressure node, the reflection coefficient at this current point is $-e^{-2j\omega T}$.

References

- Anderson, A.B.C., 1953. A circular-orifice number describing dependency of primary Pfeifenton frequency on differential pressure, gas density and orifice geometry. *Journal of the Acoustical Society of America* 25, 626–631.
- Archer, A., Boyer, A., Nimanbeg, N., L'Exact, C., Lemerrier, S., 2002. Résultats des essais hydrauliques et hydroacoustiques du tronç on PTR 900 sur la boucle EPOCA (in French). EDF R&D, Technical Note HI-85/02/023/A, France.
- Au-Yang, M.K., 2001. *Flow-Induced Vibration of Power and Process Plant Components: A Practical Workbook*. ASME Press, New York.
- Ball, J.W., Tullis, J.P., Stripling, T., 1975. Predicting cavitation in sudden enlargements. *ASCE Journal of the Hydraulics Division* 101, 857–870.
- Bendat, J.S., Piersol, A.G., 1986. *Random Data—Analysis and Measurement Procedures*, second ed. Wiley-Interscience, New York, ISBN 0-471-04000-2.
- Bistafa, S.R., Lauchle, G.C., Reethof, G., 1989. Noise generated by cavitation orifice plates. *ASME Journal of Fluids Engineering* 111, 278–289.
- Blake, W.K., 1986. *Mechanics of Flow-Induced Sound and Vibration*, vol. II. Academic Press, Orlando.
- Blake, W.K., Powell, A., 1983. The development of contemporary views of flow-tone generation. In: *Recent Advances in Aeroacoustics*, Springer, New York.
- Blevins, R., 1984. *Applied Fluid Dynamics Handbook*. Krieger, New York ISBN 0-89464-717-2.
- Bodén, H., Abom, M., 1986. Influence of errors on the two-microphone method for acoustic properties in ducts. *Journal of the Acoustical Society of America* 79 (2).
- Brennen, C.E., 1995. *Cavitation and Bubble Dynamics*. Oxford University Press, Oxford.
- Caillaud, S., Gibert, J.R., Moussou, P., Cohen, J., Millet, F., 2006. Effect on pipe vibrations of cavitation in an orifice and in globe-style valves. In: *ASME Pressure Vessels and Piping Division Conference, Proceedings PVP2006-ICPVT11-93882*, Vancouver, Canada.
- Davies, P.O.A.L., Bhattacharva, M., Bento Coelho, J.L., 1980. Measurement of plane wave acoustic fields in flow ducts. *Journal of Sound and Vibration* 72, 539–542.
- Durrieu, P., Hofmans, G., Ajello, G., Boot, R., Aurégan, Y., Hirschberg, A., Peters, M.C.A.M., 2001. Quasisteady aero-acoustic response of orifices. *Journal of the Acoustical Society of America* 110 (4), 1859–1872.
- Esipov, I.B., Naugol'nykh, K.A., 1975. Cavitation noise in submerged jets. *Soviet Physics Acoustics* 21, 404–405.
- Fletcher, N.H., 1979. Excitation mechanisms in woodwind and brass instruments. *Acustica* 43, 63–72.
- Franc, J.P., Avellan, F., Belahadjji, B., Billard, J.Y., Briançon-Marjollet, L., Fréchou, D., Fruman, D.H., Karimi, A., Kueny, J.L., Michel, J.M., 1999. *La cavitation* (in French). ISBN 2.7061.0605.0, Presses Universitaires de Grenoble.
- Franklin, R.E., McMillan, J., 1984. Noise generation in cavitating flows, the submerged jet. *ASME Journal of Fluids Engineering* 106, 336–341.
- Gilbarg, G., 1960. Jets and cavities. In: Pflügge, S. (Ed.), *Handbuch der Physik*, vol. 9. Springer, Berlin, pp. 311–445.
- Hassis, H., 1999. Noise caused by cavitating butterfly and monovar valves. *Journal of Sound and Vibration* 225, 515–526.
- Idel'cik, I.E., 1969. *Memento des pertes de charge* (in French). Eyrolles, Paris.
- Jorgensen, D.W., 1961. Noise from cavitating submerged water jets. *Journal of the Acoustical Society of America* 33 (10), 1334–1338.
- Keller, A.P., 1994. New scaling laws for hydrodynamic cavitation inception. In: *Second International Symposium On Cavitation*, vol. 2, Tokyo, Japan, pp. 327–334.
- Kim, B.C., Pak, B.C., Cho, C.H., Chi, D.S., Choi, H.M., Choi, Y.M., Park, K.A., 1997. Effects of cavitation and plate thickness on small diameter ratio orifice meters. *Flow Measurement and Instrumentation* 8, 85–92.

- Kugou, N., Matsuda, H., Izuchi, H., Miyamoto, H., Yamazaki, A., Ogasawara, M., 1996. Cavitation characteristics of restriction orifices. ASME Fluids Engineering Division Conference, FED-vol. 236 (1), San Diego, California, pp. 457–462.
- Latorre, R., 1997. Bubble cavitation noise and the cavitation noise spectrum. *Acta Acustica* 83, 424–429.
- Lecoffre, Y., 1994. La cavitation, traqueurs de bulles (in French). Hermes, Paris, ISBN 2-86601-409-X.
- Lighthill, J., 1978. *Waves in Fluids*. Cambridge University Press, Cambridge.
- Martin, C.S., Medlarz, H., Wiggert, D.C., Brennen, C.E., 1981. Cavitation inception in spool valves. *ASME Journal of Fluids Engineering* 103, 564–576.
- Morfe, C.L., 1971. Acoustic energy in non-uniform flows. *Journal of Sound and Vibration* 14, 159–170.
- Moussou, P., 2005. An attempt to scale the vibration of water pipes. Proceedings 71217 of PVP, ASME, Denver, Colorado, USA.
- Moussou, P., Caillaud, L., Villouvier, V., Archer, A., Boyer, A., Rechu, B., Benazet, S., 2003. Vortex-shedding of a multi-hole orifice synchronized to an acoustic cavity in a PWR piping system. In: PVP-vol. 465, Flow-Induced Vibration PVP2003-2086, ASME Press, New York, pp. 161–168.
- Moussou, P., Cambier, C., Lachene, D., Longarini, S., Paulhiac, L., Villouvier, V., 2001. Vibration investigation of a French PWR power plant piping system caused by cavitating butterfly valves. In: PVP-vol. 420–2, Flow-Induced Vibration: Axial Flow, Piping Systems, Other Topics, ASME Press, New York, pp. 99–106.
- Moussou, P., Lafon, Ph., Potapov, S., Paulhiac, L., Tijsseling, A., 2004. Industrial cases of FSI due to internal flows. In: Ninth International Conference on Pressure Surges, Chester (UK), vol. 1. pp. 167–184, BHR Group Limited.
- Numachi, F., Yamabe, M., Oba, R., 1960. Cavitation effect on the discharge coefficient of the sharp-edged orifice plate. *ASME Journal of Basic Engineering* 82, 1–11.
- Pan, S.S., Xiang, T., Wu, B., 2001. Investigating to cavitation behavior of orifice tunnel. CAV2001, Fourth Symposium on Cavitation, California Institute of Technology, Pasadena, USA (<http://cav2001.library.caltech.edu/222>).
- Pierce, A.D., 1981. *Acoustics: An Introduction to its Physical Principles and Applications*. McGraw-Hill Book Company Inc., New York.
- Rockwell, D., Naudascher, E., 1979. Self-sustained oscillations of impinging free shear layers. *Annual Review of Fluid Mechanics* 11, 67–94.
- Sato, K., Saito, Y., 2001. Unstable cavitation behavior in a circular–cylindrical orifice flow. CAV2001, Fourth Symposium on Cavitation, California Institute of Technology, Pasadena, USA (<http://cav2001.library.caltech.edu/318>).
- Tullis, J.P., 1989. *Hydraulics of Pipelines: Pumps, Valves, Cavitation, Transients*. Wiley Interscience Ed., New York.
- Tullis, J.P., Govindajaran, R., 1973. Cavitation and size scale effects for orifices. *ASCE Journal of the Hydraulics Division* 99, 417–430.
- Van Wijngaarden, L., 1972. One-dimensional flow of liquids containing small gas bubbles. *Journal of Fluid Mechanics* 16, 369–396.
- Verge, M.P., 1995. *Aeroacoustics of confined jets*. Thesis, Technische Universiteit Eindhoven, The Netherlands, ISBN-90-386-0306-1.
- Weaver, D.S., Ziada, S., Au-Yang, M.K., Chen, S.S., Padoussis, M.P., Petitgrew, M.J., 2000. Flow-induced vibration of power and process plant components: progress and prospects. *ASME Journal of Pressure Vessel Technology* 122, 339–348.
- Yan, Y., Thorpe, R.B., 1990. Flow regime transitions due to cavitation in the flow through an orifice. *International Journal of Multiphase Flow* 16 (6), 1023–1045.
- Yan, Y., Thorpe, R.B., Pandit, A.B., 1988. Cavitation noise and its suppression by air in orifice flow. In: *Symposium on Flow-Induced Noise*, Chicago, Ill., vol. 6. ASME, New York, pp. 25–39.
- Young, F.R., 1999. *Cavitation*. Imperial College Press, London ISBN 1-86094-198-2.